Heliyon 10 (2024) e24311

Contents lists available at ScienceDirect

Heliyon

journal homepage: www.cell.com/heliyon

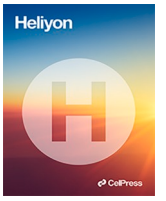

Research article

Assessment of the impact of rainfall uncertainties on the groundwater recharge estimations of the Tikur-Wuha watershed, rift valley lakes basin, Ethiopia

Tsegamlak Diriba Beyene [a,d,*], Fasikaw Atanaw Zimale [a,b], Sirak Tekleab Gebrekristos [c], Dessie Nedaw [a,e]

[a] Africa Center of Excellence for Water Management, Addis Ababa University, Addis Ababa, Ethiopia
[b] Faculty of Civil and Water Resources Engineering, Bahir Dar Institute of Technology, Bahir Dar University, Bahir Dar, Ethiopia
[c] Ethiopian Institute of Water Resources, Addis Ababa University, Addis Ababa, Ethiopia
[d] School of Hydraulic and Water Resources Engineering, Dilla University, Dilla, Ethiopia
[e] School of Earth Sciences, Addis Ababa University, Addis Ababa, Ethiopia

ARTICLE INFO

Keywords:
Groundwater
Recharge
Uncertainty
WetSpa
Tikur-wuha

ABSTRACT

Spatial recharge estimation uncertainty is directly proportional to uncertainty in input precipitation data Thus, the main objective of this study was to investigate the recharge uncertainty by using improved spatial rainfall observations. The physically based fully distributed hydrological model WetSpa was used to simulate 20,000 possible combinations of parameters for two model setup. The M_1 model setup was developed based on the rainfall measurements obtained from rain gauge stations scattered in and around the Tikur-Wuha watershed in Ethiopia, while M_2 model setup was developed using bias-corrected satellite rainfall estimates (SREs) based on Climate Hazards Group InfraRed Precipitation (CHIRP) merged with relevant ground station records. The required parameter combinations were generated using Monte Carlo simulation stratified by applying Latin Hypercube Sampling (LHS). One hundred best performing parameter combinations were selected for each model to generate spatial recharge statistics and assess the resulting uncertainty in the recharge estimates. The results revealed that enhanced spatial recharge estimates can be produced through improved CHIRP-based SREs. The long-term mean annual recharge (218.29 mm) in the Tikur-Wuha watershed was estimated. Model parameter calibration performed using discharge measurements obtained from the Wosha rain gauge station located in the subcatchment area of the Tikur-Wuha watershed had a Nash-Sutcliffe efficiency of 0.56. Seventy percent of the watershed showed a coefficient of variation (Cv) < 0.15 for M_2, while 90 % of the area exhibited a Cv < 0.15 for M_1. Furthermore, the study findings highlighted the importance of improving evapotranspiration data accuracy to reduce the uncertainty of recharge estimates. However, the uncontrolled irrigation water uses and the total recharge coming from the irrigation fields scattered across the Tikur-Wuha watershed were not considered in the study, which is a limitation of the study. Future studies should consider the contribution made by irrigation water to the total recharge of the watershed.

* Corresponding author. Africa Center of Excellence for Water Management, Addis Ababa University, Addis Ababa, Ethiopia.
E-mail addresses: tsegamlak.diriba@aau.edu.et (T.D. Beyene), fasikaw@gmail.com (F.A. Zimale), siraktekleab@yahoo.com (S.T. Gebrekristos), dessienedaw@yahoo.com (D. Nedaw).

https://doi.org/10.1016/j.heliyon.2024.e24311
Received 25 June 2023; Received in revised form 19 December 2023; Accepted 5 January 2024
Available online 9 January 2024

1. Introduction

Sustainable water resources management requires the modeling of hydrological cycle components with minimum error. One key component of the water cycle is the estimation of groundwater recharge. However, in hydrogeological modeling, various sources can cause estimation uncertainties. The main sources of estimation uncertainties are the input, structure, and the parameters of the model used [1]. Groundwater recharge, variable both spatially and temporally, is highly influenced by climate variables, land use/cover, and soil distribution [2]. Among the three influencing factors, climate variables and land use/cover, considered as direct inputs in most hydrological modeling approaches, are temporal variables, and thus an in-depth assessment of their contribution to uncertainties in groundwater recharge estimation has become necessary.

Considering the significant contribution made by input data to groundwater recharge estimation uncertainties, Ampe et al. (2012), investigated recharge estimation uncertainties using two land-use classification methods [3]. Their study findings revealed that the recharge estimates produced for the Woluwe river catchment in Belgium based on pixel-based land-use classifications are more uncertain compared with those produced using region-based classifications [3]. Abraham et al. (2022) who studied the wetland-dominated Tikur-Wuha watershed explored the uncertainty and sensitivity associated with land-use maps [4]. In their study, wetland parameter was introduced in the Soil Water Assessment Tool with Calibration and Uncertainty Program (SWAT-CUP), a hydrological model, through which the uncertainties because of land-use maps were quantified using the sequential uncertainty fitting interval algorithm SUFI-2. The study proved that the quality of groundwater recharge estimation can be improved by considering multiple land-use maps to ensure that land use/cover changes are incorporated. Ampe et al. (2012) and Zomlot et al. (2017) also made similar conclusions [3,5]. The uncertainty of recharge from irrigation fields and canals along with six other parameters was investigated by Baker et al. (2022) [6]. The findings indicated that 91 % of the aquifer recharge was contributed by irrigation water from rice fields and leakage from canals.

The impact of the evapotranspiration time series on the uncertainty in recharge was studied by Xie et al. (2018) [7]. The study revealed that recharge uncertainty can be reduced by up to 50 % for improved evapotranspiration observations and that an insignificant reduction in recharge estimation could be obtained by using distributed soil moisture time-series data. Other hydrological simulations can also be performed using satellite-based evapotranspiration estimates [8]. Dile, Yihun T et al. (2020) emphasized that data scarce areas could particularly benefit from using satellite estimates because of reduced errors [8]. Duan et al. (2019) showed that the performance of satellite-based estimates are low when compared to performance of evenly and adequately collected temperature and precipitation ground records [9].

Spatial recharge estimation uncertainty is directly proportional to the uncertainty in precipitation data used in the estimation process [7,10,11]. The statistical characteristics of rainfall and reference evapotranspiration dataset used in recharge estimation were studied by Turkeltaub and Bel (2023) for the semiarid climate regions in China and Israel [12]. The findings indicated that spatial local rainfall and the reference evapotranspiration dataset can significantly influence recharge estimation [12]. Thus, improved spatial precipitation estimates can minimize the uncertainties in recharge estimations. The availability of improved spatial precipitation data, such as those obtained through radar, rain gauge observations, satellite observations, and reanalysis products, is increasing significantly [13,14]. The importance of using satellite rainfall products for minimizing hydrological modeling errors has been assessed in previous studies [15,16]. Such assessments are particularly important for complimenting the scanty observation made in developing countries [17].

Rainfall records are scarce in Ethiopia and are mostly available for locations along the main road routes [17,18]. Development activities requiring quality rainfall records are hindered in rural areas because of the scarcity or unavailability of accurate rainfall records [18,19]. Satellite technology developments in the past few decades have contributed for improving the observation and measurement of several meteorological parameters. Nevertheless, eliminating the errors in most meteorological measurements is challenging. However, merging multiple sources of records will help capture the merits of each source and thereby reduce the errors in groundwater recharge estimations [20].

Previous studies [4,21,22] have shown that agricultural land use/cover of the Tikur-Wuha watershed has increased significantly. This once wetland-dominated watershed is now losing its coverage to grasslands and agriculture. A recent study by Abraham et al. (2022) showed that median annual recharge in Tikur-Wuha has reduced from 506.25 to 483.34 mm [4]. Thus, urgent changes to water resources management regulations and practices supported by accurate estimates of groundwater recharge have become necessary. Multiple studies [21,23–26] have quantified the recharge to the aquifers of the Hawassa watershed. However, the discrepancies in the recharge estimates presented in those studies show a high level of uncertainty in the recharge estimations. Thus, the main objective of this study was to assess the uncertainty in the recharge estimation using improved spatial rainfall observations. In the study, a bias-corrected satellite rainfall product based on Climate Hazards Group InfraRed Precipitation (CHIRP) was used along with ground observations, and the rainfall records available were converted to areal rainfall records using the conventional Thiessen polygon method.

2. Study area description

2.1. Location and topography

The Tikur-Wuha watershed covers an area of 670 km^2. It is the only perennial river flowing into Lake Hawassa. Steep mountain ranges cover the northeastern and southeastern parts of the watershed, while gently sloping land covers the north–west to south–west

parts of the watershed. Nine perennial streams feed the wetland located at the center of the watershed and the Tikur-Wuha river drains to Lake Hawassa through that wetland (Fig. 1).

The Tikur-Wuha watershed is located at 60°48′00″–70°10′00′′N latitude and 38°26′30″–38°43′00′′E longitude. It is at an elevation between 1643 and 2976 m above mean sea level. According to Mohammed et al. (2020), 54 % and 21.6 % of the Tikur-Wuha watershed have slopes ranging from 8 % to 30 %, and 3 %–8 %, respectively, while 3 % and 19 % of the watershed have slopes <3 % and >30 %, respectively [27].

2.2. Climate and hydrology

2.2.1. Climate

The Tikur-Wuha catchment has a tropical subhumid climate (Moist Weyna Dega). Its mean annual rainfall ranges from 954.5 mm in its western and northwestern parts (low lands) to 1152.5 mm in its southeastern part (mountainous section of the catchment). As reported by Belete et al. (2017), up to 70 % of the annual rainfall in Ethiopia occurs when the intertropical convergence zone (ITCZ) lies over northern and southern Ethiopia from June to September [28]. The seasonal rainfall cycle, characterized as a bimodal cycle [29], is mainly controlled by the movement of the ITCZ [28].

The seasonal rainfall in the watershed can be quantified as follows: Thirty percent of the annual rainfall occurs between March and May with the seasons from June to September and October to February contributing 50 % and 20 % of the rainfall, respectively [28]. The average maximum and minimum temperatures of the watershed range from 11 to 20 °C, and the hottest dry month of the watershed is March [30].

2.2.2. Hydrology

Tikur-Wuha subwatershed is located within the geographically closed watershed of Lake Hawassa, where uncontrolled irrigation practices are on the increase. The Tikur-Wuha river feeds Lake Hawassa and the water from the Tikur-Wuha watershed meets the water requirements of households, livestock, irrigation, industries, and the environment. Nine streams, namely Bele-Lango, Wesha, Werka, Hallo, Shenkora, Gomesho, Wedesa, Abosa, and Gelchacha, flow through the Tikur-Wuha watershed, which drains to the Cheleleka wetland [31]. The aggravated land cover changes have resulted in the disappearance of one lake within the Cheleleka wetland [32]. The Cheleleka wetland exhibits flow stabilizing properties by serving as an intermediary between the upper catchments of the nine rivers, where the water flow is rapid, and the Tikur-Wuha river, where the water flow is slow. The wetland receives the water from the nine streams and channels it to one outlet to feed the Tikur-Wuha river, which then drains into Lake Hawassa. The watershed outlet is located at the Tikur-Wuha bridge. The watershed covers an area of 645.75 km^2, and the estimated average annual flow of the river for the period between 1987 and 1996 is 132.6 mm, calculated by dividing the average annual stream flow volume by the total area of the watershed [4,29].

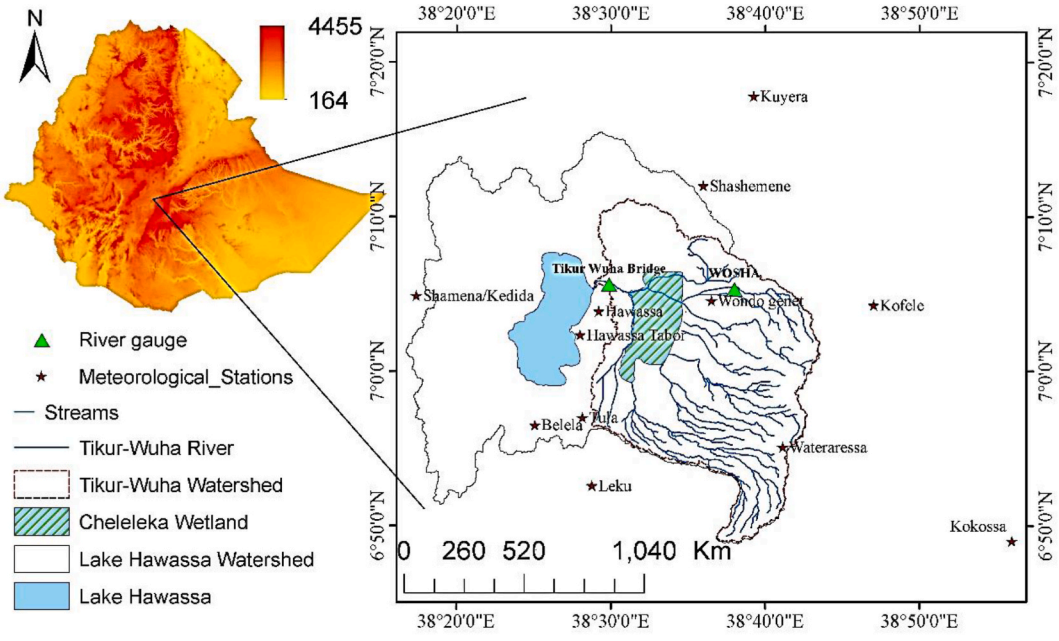

Fig. 1. Location map of the study area.

2.3. Land use and soil

Studies focusing on land use/cover classifications have shown that since the year 2000 -, a majority of the watersheds have become cropland used for small scale plantations, rain-fed crop fields, and perennial cash crops. According to Wondrade et al. (2014), between 1973 and 2011, the cropland coverage has increased by 12.8 % [32]. Other major types of land use/cover in the watershed includes grasslands, wetland, forests, urban areas, and shrub land. Most of the forest cover is in the escarpments, and the rift floor is covered with wet land, grasslands, and cropland. A significant change that has occurred in the land use/cover dynamics is the disappearance of Lake Cheleleka, which covered 1300 ha [32]. The disappearance of Lake Cheleleka can be attributed to environmental degradation due to extensive deforestation, climate change, and other anthropogenic stressors [32]. However, no studies have been conducted to particularly investigate the real causes that led to the disappearance of the lake. In general, 73.4 % of the watershed has experienced land use/cover changes between the years 1972 and 2017 [33].

The soil map of the watershed (Fig. 3) indicates that sand, clay loam, sandy loam, and silt soil cover 17.24 %, 24.78 %, 51.01 %, and 17.10 % of the watershed, respectively. According to Mohammed et al. (2020), Leptosol, Vertic cambisol, Vertic Luvisol, Vitric Andosol, Haplic Luvisol, and Eutric Cambisol are the major types of soil found in the Tikur-Wuha watershed with Vertic Luvisol and Haplic Luvisol dominating 39.6 % and 39.2 % of the watershed, respectively [27].

The geological map of the study area (Fig. 2) shows the presence of densely populated normal faults in the southeastern part of the watershed. The drainage pattern of the study area (Fig. 1) overlaid on its geological map showing fault lines (Fig. 2) indicates that most of the fault lines intersect the main drainage lines to form point recharges, which have the potential to increase surface flow interception. Ayenew and Tilahun (2008) argued that simulations conducted during severe faulting should consider fractured volcanic aquifers as porous mediums, enabling the heavily fractured regions to exhibit high hydraulic conductivities [23]. Their study also highlighted that the existing fault structures and newly emerging cracks have the potential to create point recharges.

3. Methodology

3.1. Datasets

The chosen WetSpa model (Table 1) has as its inputs such as land-use map, soil map, digital elevation model (DEM) and hydrometeorological data. Because the aim of this study was to assess the recharge estimation uncertainties associated with rainfall data, two sets of rainfall records were used. The first rainfall record set contained point observations made using rain gauges located in and

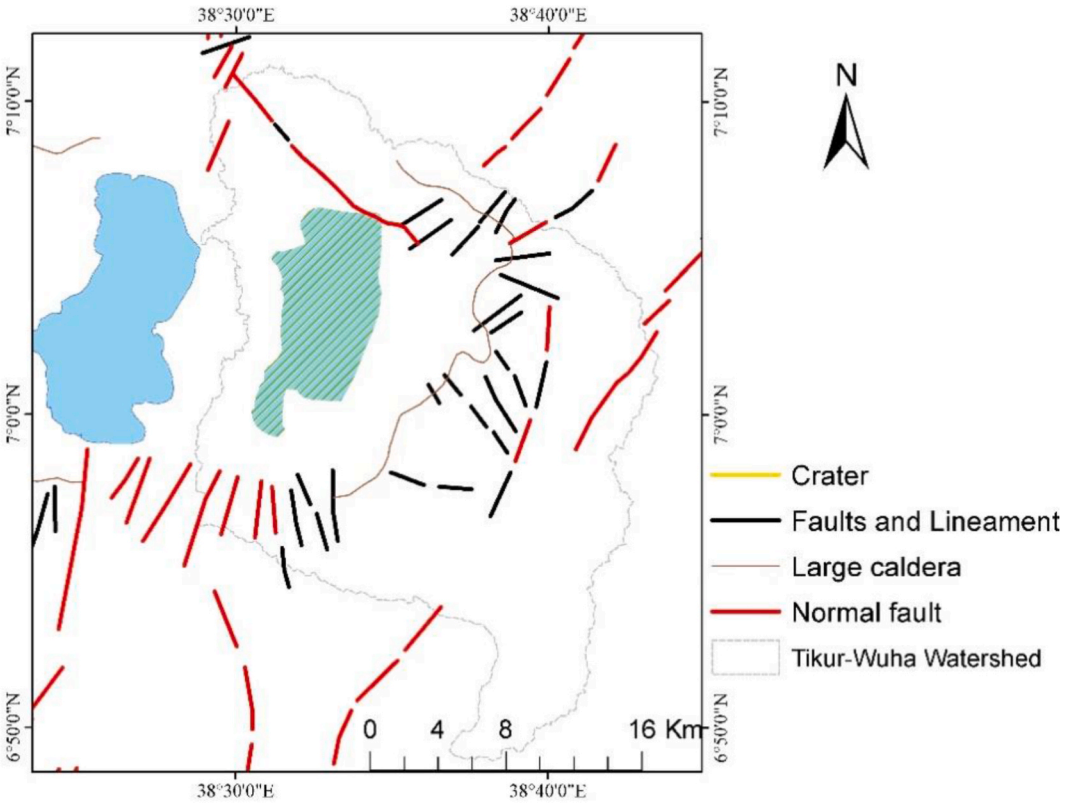

Fig. 2. Structural geology of the study area.

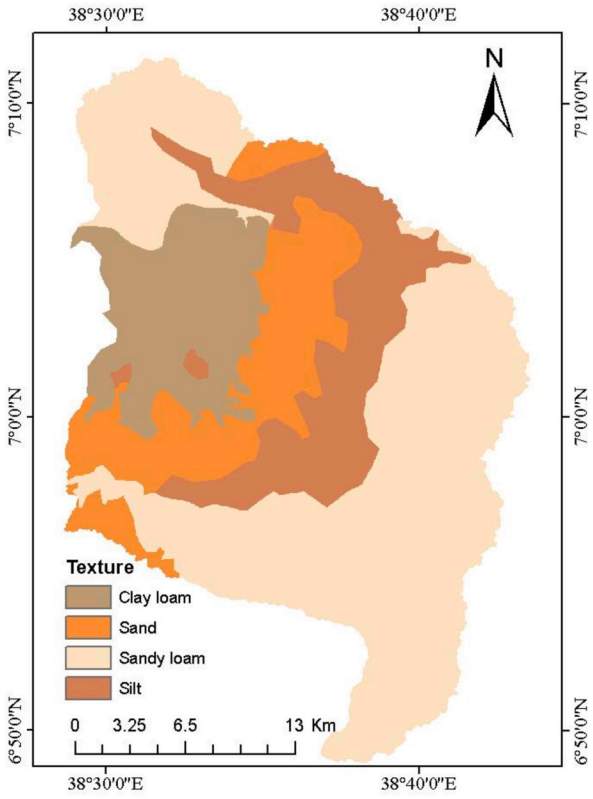

Fig. 3. Soil texture map of the study area.

around the watershed, whereas the second rainfall record set was obtained by combining the satellite rainfall product CHIRP with station data and available ground station records.

3.1.1. Meteorological data

The required meteorological parameters were gathered from the stations located near the Lake Hawassa watershed. Daily meteorological records of two synoptic meteorological stations, two ordinary meteorological stations, and eight rain gauges were obtained from the National Ethiopian Meteorological Agency. Synoptic meteorological stations measure precipitation, wind speed, sunshine duration, maximum and minimum air temperatures, and relative humidity, at 15 min intervals. Alternatively, ordinary meteorological stations record only the precipitation, and maximum and minimum air temperatures. The remaining stations provide only the precipitation records.

The freely available CHIRP was downloaded from https://data.chc.ucsb.edu. It is a satellite rainfall product that provides daily rainfall estimates at a grid scale of 0.05° [34]. A merged rainfall dataset was prepared based on the records obtained from 11 stations [35]. However, records from only five stations were available for the year 2005, while records from only eight stations were available for the year 2006. Furthermore, for estimating the areal rainfall in the Tikur-Wuha watershed using the conventional Thiessen polygon method, the records from only four stations located in and around the watershed were used.

Grubbs and Beck test, Mann–Whitney test, Wald-Wolfowitz test, and double mass analysis were used to assess the outliers, homogeneity and stationarity, independence and stationarity, and consistency, respectively, of the meteorological data records. The rainfall data obtained from the Hawassa and Shashemene stations exhibited only slight deviations from the historical record, whereas the rainfall data obtained from the Wateraresa station exhibited significant deviations from the historical record requiring corrections

Table 1
Input data sets and their respective data sources.

Data Description	Source	Detail	Time scale
Ground Meteorological time-series data	National Ethiopian Meteorological Agency	2005–2014	daily
CHIRP satellite rainfall estimates (SRE)	https://data.chc.ucsb.edu	2005–2014	daily
Digital elevation model	http://gdex.cr.usgs.gov/gdex/	30 m resolution	–
Soil map	Geological Survey of Ethiopia	–	–
Daily stream flow data	Ministry of water and energy of Ethiopia	@Wosha 2005–2014	daily
		@Dato-village 2005–2014	daily

for consistency. Other quality tests were also conducted on sample data obtained from each station to ascertain the daily maximum air temperatures, and their annual values. The tests conducted for independency, homogeneity, and stationarity indicated that the data obtained were homogeneous and independent. The arithmetic mean method was used to fill missing data records. Moreover, based on the results of analyzing the quality of rainfall data obtained from different stations, rainfall records obtained from the Shashemene station were not considered in the modeling process.

Evapotranspiration time-series data were also required by the WetSpa model used to simulate stream flow. The assessment results of the meteorological records of the stations in and around the watershed indicated that temperature-based evapotranspiration estimates would effectively represent the spatial variability of evapotranspiration. Accordingly, a simple temperature method (Eq. (1)) developed by Enku and Melesse (2014) was used to estimate evapotranspiration [36]. However, because of the differences in the time periods over which the data from different stations were recorded, only temperature data obtained from the Hawassa, Wateraressa, and Kofele stations were used in the estimation.

$$ET_o = \frac{(T_{max})^n}{k} \tag{1}$$

where ET_o is the reference evapotranspiration (mm day^{-1}), T_{max} is the maximum daily temperature (^{o}C), n is a coefficient equal to 2.5, and k is a coefficient, equal to 48*T_mm-330, 73*T_mm-1015, and 38*T_mm-63 for dry and wet seasons combined, dry seasons, and wet seasons, respectively. T_{mm} is the long-term daily mean maximum temperature for the seasons under consideration (^{o}C), where T_{mm} is calculated by taking the maximum of long-term daily mean temperature records for a specified season.

3.1.2. Spatial datasets

A 30-m resolution DEM was sourced from http://gdex.cr.usgs.gov/gdex/and resampled to a 32-m resolution to be fed to the WetSpa model. The other spatial inputs fed to the model included the soil and land use/cover maps of the watershed. The soil map of the Tikur-Wuha watershed (Fig. 3) was obtained from the Ethiopian Institute of Geological Surveys. The land use/cover map was prepared using LandSat-8 images for 2014 and classified using Google Earth Engine. Although the land-use map of the watershed has significantly changed since 2014, it was assumed to be applicable to the simulation period from 2005 to 2014. The pixel resolution of the land use/cover raster map and reference systems of all spatial datasets were kept constant. A pixel resolution of 32 m was used in the land use/cover raster map and a Universal TransverseMercator (UTM) Zone 37 N was used as the reference system for the land use/cover spatial datasets.

3.1.3. Stream flow datasets

As already explained, the Tikur-Wuha watershed has nine streams feeding the Cheleleka wetland. However, only two hydrological gauging stations are available at the Tikur-Wuha watershed. Two gauging stations are located at the Tikur-Wuha river, downstream of the Cheleleka wetland. The first Tikur-Wuha river gauging station is stationed at the bridge near the inlet of Lake Hawassa and the second Tikur-Wuha river gauging station, called Dato-village station, is located upstream of the bridge. The rainfall records of the first gauging station are available for the year preceding 2005. During peak flood periods, the back flow from the lake affects the stream flow records. Currently, the area where the bridge is located is completely covered with vegetation, making the gauging station nonfunctional. However, the back water flowing from the lake during peak flood seasons does not reach the Dato-village station. Thus, the back flow will have no effect on the records maintained at the Dato-village station. The physical inspection of the station location and analysis of the back water effects, which is not presented here, indicate that the Dato-village station has not been affected by back

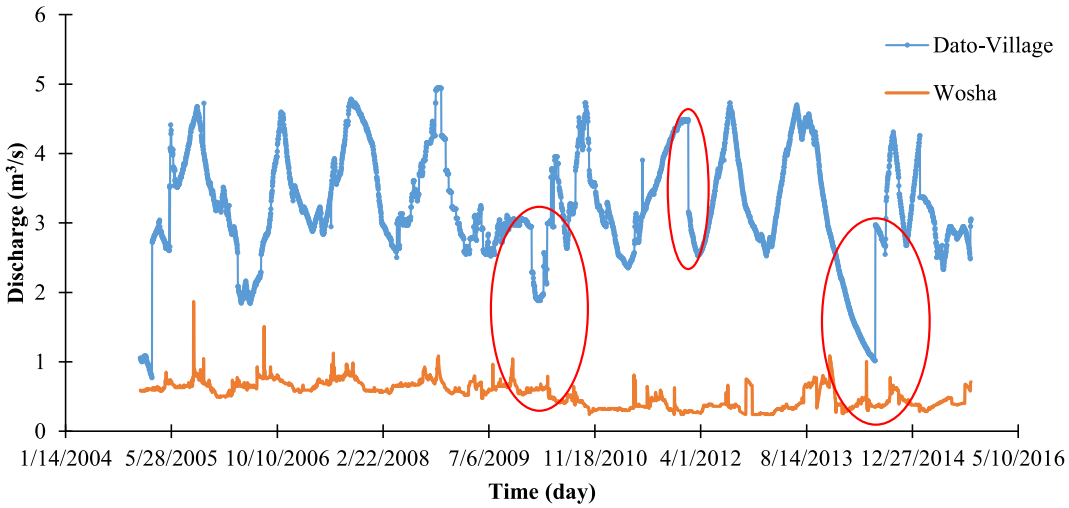

Fig. 4. Discharge time-series data.

water during flooding seasons. Thus, the discharge records of the Dato-village station were used in this study for calibration purposes.

Discharge records were also available at the Worka and Wosha stations situated in the Tikur-Wuha subwatershed. The discharge measurements have been made at the Worka station only in the year preceding 2005, and thus had to be disregarded. Thus, the records maintained at the Wosha station (Fig. 4) were used for the calibration of parameters along with the records of the Dato-village station.

Although the Wosha River is a tributary of the Tikur-Wuha river, the flow patterns of the two rivers vary, determined by comparing their flow records. The in-depth observation of the discharge time series (Fig. 4) revealed that the peak and low flows are not similar in some sections of the records, as indicated by the red circles in Fig. 4. Additionally, the sharp fall of the falling limb and sharp rise of the rising limb, of the Tikur-Wuha river hydrograph makes the modeling challenging to capture the flow pattern fully.

3.2. Methods

3.2.1. General method

Uncertainties of the rainfall data were first quantified by creating two separate model setups. This quantification was achieved by having similar inputs to the selected hydrological models and by changing the input rainfall time series. The input time series to the first model setup (M_1), prepared from the available rain gauge records, was subsequently converted into areal rainfall by using the Thiessen polygon. The rainfall data fed to the second model setup (M_2) were prepared by applying first-order bias correction (using empirical parametric quantile mapping) to the CHIRP-based SREs followed by their merging with the available rain gauge data using a conditional merging technique.

In the next step, the global parameters of the two hydrological models were set based on prior watershed knowledge and literature review findings. Monte Carlo simulation in conjunction with Latin Hypercube Hampling was conducted to generate 10,000 possible parameters (i.e., WetSpa model parameters) using R programming. A second semidistributed model simulation using all possible parameter combinations in each model setup was performed to determine model performance in terms of root mean squared error (RMSE) and percent error of volume (PVE). In the third step, the long-term mean recharge was quantified for each accepted model realization followed by analysis of the statistical long-term mean recharge distribution.

Only daily time-step simulation could be conducted for 10 consecutive years (2005–2014) because of the scarcity of overlapping hydrometeorological data. From the accepted model realizations, 100 best parameter combinations were selected and a distributed model simulation was performed using each model setup. The 100 recharge maps obtained from each model setup were then used to obtain spatial statistics and related uncertainties of the recharge estimations. A fully distributed simulation model was expected to run 1,113,264 analyses for a 32-m resolution map. A computer with 128 GB RAM and 9 processors took 24 h to complete a single run. Thus, the number of simulations that could be performed was limited owing to computer capacity constraints. Furthermore, Xie et al. (2018) shows that 10,000 simulations run with each model setup would ensure acceptable variability in parameter combinations [7]. The simulations run with each semidistributed model setup were automated using Python programming, whereas only manual simulations were run with the fully distributed model.

The semidistributed model simulation produced water balance components at a daily time step, whereas the fully distributed model simulation produced a gridded recharge map for a 10-year simulation period. Thus, the long-term mean annual recharge had to be determined for each semidistributed model simulation by first aggregating the daily recharge for each year and then averaging it, for the fully distributed model simulation, each cell was divided by the length of the simulation period to obtain the mean annual recharge for each simulation.

3.2.2. Land use/cover classification

From the LandSat-8 image of the study area, the land-use map of the area was developed for the year 2014 by employing supervised classification using Google Earth Engine, freely available at https://developers.google.com/earth-engine/guides/classification. The supervised classification procedure involves screening images for cloud cover, correcting them for surface reflectance, identifying training points (ground truth points) for each land-use type, and finally classifying the land use. The selected training points were randomly split into two sets as calibration and validation sets, and the SMILE Random Forest classifier [37] provided in the Google Earth Engine was used for land-use classification. The adopted code used used to compute the training and validation accuracies. A confusion matrix representing substitution accuracy was produced and the Kappa coefficient was calculated to assess the land-use classification accuracy [38].

3.2.3. WetSpa model

A hydrological simulation was conducted using a physically based distributed hydrological model and the water and energy transfers between soil, plants, and atmosphere (WetSpa) were predicted at a daily time step. The WetSpa extension [39], a GIS-based distributed watershed model, was employed in this study. WetSpa simulates the hydrological processes (precipitation, interception, snowmelt, depression, infiltration, evapotranspiration, percolation, surface runoff, interflow, and groundwater flow) for each grid cell by dividing the hydrological system into four control volumes: plant canopy, soil surface, root zone, and groundwater aquifer [39].

The hydrological simulation performed using the WetSpa extension can generally be achieved in three stages. The first stage involves the determination of the local variables based on gridded DEM, soil map, and land-use map. This step was conducted using ArcView 3.2 software. All local variables were predetermined based on the information provided in the three base maps. Liu and De Smedt (2004) provide a detailed description of the preparation and running of the WetSpa extension [39]. In the second stage, the external executable is run with the extension providing a choice of fully distributed and semidistributed models.

The point rainfall records required by the WetSpa model were obtained from the rain gauge stations located in and around the

targeted watershed. The point rainfall records were converted to areal rainfall estimates using the Thiessen polygon method. When running the fully distributed model, the developed Thiessen polygon map is converted to a raster map, where the station number is the cell value. In this study, for the M_1 model setup, a similar procedure was followed to create the Thiessen polygon map using the available rain gauge stations. In the M_2 model setup, each grid cell center was assumed to represent a rain gauge station and the grid map was considered the Thiessen polygon.

3.2.4. WetSpa parameter range

WetSpa simulations (Fig. 5) are conducted at cell level, and thus for each cell, all local parameters have to be determined. A 32 x 32 resolution produced a grid mesh area with 859 columns and 1296 rows for the watershed. Default local parameters were determined by the WetSpa extension based on the input soil texture class, land-use type, and physiographic characteristics of each cell. All default parameters were retained except for the root depth of the forest, which was changed from 1 to 5 m considering the dominant presence of Eucalypts in the watershed forest cover. Similar changes were made by Yenehun et al. (2022) and Yenehun et al. (2020) when they applied WetSpass simulations to the Lake Tana basin and Gilgel Abay watershed, respectively [40,41].

Eleven global parameters (Table 2) were used to calibrate the model that simulated runoff hydrograph at Tikur-Wuha watershed outlet [39]. Three of the parameters, namely base snowmelt temperature (To), temperature degree-day coefficient (k-snow), and rainfall degree-day coefficient (k-rain), were used to control the snow melt [42]. For regions with no snowing, each of these parameters can be set to −1.0 [39]. Similar adjustments were made by Kidanemariam et al. (2021) presuming that no significant snow formation occurred in the targeted basin [43]. The ability to adjust slightly sensitive or insensitive parameters comes as an added advantage when narrowing down the feasible parameter range [44]. The initial soil moisture condition (K-s), which affects only the initialization period of the simulation, is also a slightly sensitive parameter [42].

Other parameters can also be assigned to the model, based on the physical and meteorological characteristics of the targeted watershed [44]. Accordingly, the base flow recession curve coefficient (Kg) can be determined from the slope of the master curve of the recession limbs; observed precipitation can be used to determine the feasible range of the correction factors used for maximum precipitation (P-max), potential evapotranspiration (K-ep), and surface runoff exponent for a zero rainfall intensity (k-run). Moreover, the cumulative flow curve can indicate the feasible maximum groundwater level (g-max), while the annual rainfall can indicate initial ground water storage (g0) [42]. Finally, the scaling factor for the inter flow (Ki) could be set by considering the most dominant land-use class of the watershed [42].

3.3. Performance measures

Choosing statistical performance indicators in a study is highly subjective and should be orientated based on the intended purpose of the study [45]. The performance of each simulation model was determined using the daily stream flow at the watershed outlet. The estimated evapotranspiration was also used as a performance measure. The two statistical performance measures RMSE and PVE were also used. The range of the PVE is from $-\infty$ to $+\infty$. The results falling within the range between −10 % and +10 % indicate satisfactory performance, whereas the results falling outside that range indicates poor performance, with 0 representing perfect performance. PVE (Eq. (2)), which considers the computed volume, does not account for the peak magnitude as indicated below.

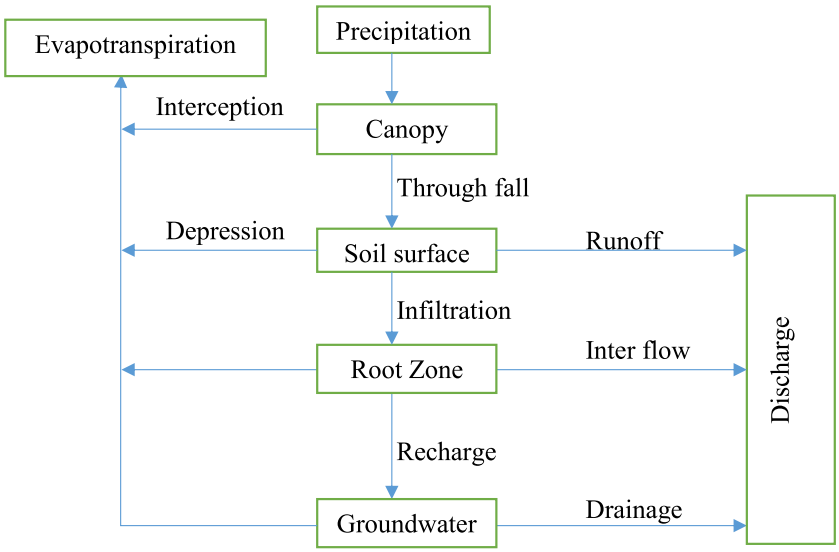

Fig. 5. WetSpa simulation at grid cell level [39].

Table 2
WetSpa global parameter ranges.

Parameter	Range	Description
Ki	1.5–2.2	Seasonally vegetated farm lands and commercial mixed forest are the dominant land covers
Kg	0.0001–0.0003	Based on the recession curve of observed hydrograph
K-s	1.0–1.2	Assuming up to 20 % influence of initial soil moisture condition
K-ep	0.65–0.95	Based on the assumption that can represent seasonal variability
g0	1000–1900	Based on the observed annual rainfall amount
g-max	1000–5100	Based on the assumed maximum root depth
k-run	7.5–10.5	The observed hydrograph has low noises
P-max	100–200	Based on the maximum observed rainfall and error factors

$$PVE = 100\left|\frac{Vo - Vs}{Vo}\right| \tag{2}$$

where: PVE is the percentage error in volume, *Vo* is the observed volume, and *Vs* is the simulated volume.

The error variation between raw and bias-corrected SREs and ground observation can be indicated by the RMSE, which falls within the range between 0 and ∞. If the RMSE (RMSE; Eq. (3)) is close to zero, performance would be quite satisfactory and vice versa. The mathematical representation of the RMSE is as follows:

$$RMSE = \sqrt{\frac{1}{n}\sum_{i=1}^{n}(Q_{si} - Q_{oi})^2} \tag{3}$$

where Q_{si} *and* Q_{oi} are the simulated results and ground based observations, at day i, respectively; and n is the total number of available data pairs. After calculating the performance measures for each model iteration (10,000 iterations for each of the model setups M_1 and M_2), model realizations having a PVE less than 10 % were accepted for further analysis. The errors introduced by factors such as human errors, during stream depth measurements are unavoidable. Thus, a 10 % error margin, which makes model realization with ±20 % PVE for discharge is acceptable, was considered. Additional cut-off criteria were set because the RMSEs of some model realizations were as high as 110 % of the minimum RMSE.

Calibration procedures can help to narrow down the parameter range applicable to a given watershed. Thus, Nash–Sutcliffe efficiency (NSE; Eq. (4)) was implemented during model calibration. When NSE is 1, it indicates a perfectly fitting model [45].

$$NSE = 1 - \left(\frac{\sum_{i=1}^{n}(sim - obs)^2}{\sum_{i=1}^{n}(obs - \overline{obs})^2}\right) \tag{4}$$

where − *obs* is the observed value during the i^{th} time interval; *sim* is the simulated value during the i^{th} time interval; $\overline{obs}$ is the mean of the observed parameter; and n is the total number of observations.

4. Results and discussion

4.1. Meteorological data analysis

A meteorological data analysis was conducted for the study duration, which was from 2005 to 2015. A preanalysis of the obtained

Table 3
Mean daily minimum and maximum temperature values and annual evapotranspiration values recorded at the Hawassa, Kofele, and Wateraressa rain gauge stations.

Year	Minimum Temperature (°C)			Maximum Temperature (°C)			Annual Evapotranspiration (mm)		
	Hawassa	Kofele	Wateraressa	Hawassa	Kofele	Wateraressa	Hawassa	Kofele	Wateraressa
2005	12.81	7.63	8.32	27.57	19.74	19.47	1604.96	725.13	907.20
2006	13.58	7.09	8.80	27.32	19.44	19.18	1565.69	695.45	864.64
2007	13.02	6.36	9.02	27.13	19.46	20.66	1538.42	698.02	1034.58
2008	12.86	5.40	6.13	27.27	19.72	21.09	1566.10	726.99	1101.77
2009	13.38	4.66	4.65	28.24	20.14	19.03	1697.11	760.65	854.65
2010	14.21	4.37	5.73	27.04	19.61	18.10	1522.26	707.81	758.28
2011	13.53	3.04	5.74	27.70	19.95	17.61	1623.35	745.51	715.36
2012	13.37	1.73	8.74	27.99	19.88	20.01	1668.57	741.60	958.19
2013	13.00	1.92	9.93	27.57	19.26	21.13	1602.31	681.36	1088.86
2014	13.45	8.74	10.86	27.34	19.33	21.10	1565.37	685.94	1084.88
2015	14.34	8.68	11.10	28.54	20.25	21.37	1739.46	767.73	1123.93

meteorological time-series dataset indicated that the mean annual rainfalls at the Hawassa, Wendo-Genet, Kofele, and Wateraressa stations are 954.54, 1069, 1074, and 1152 mm, respectively. The temperature records of the Hawassa station reveal that the mean daily maximum temperature at the station is more than the corresponding temperatures at the Kofele and Wateraressa stations, located within mountain ranges, by up to 10 °C. The evapotranspiration calculated from the available temperature data (Table 3) show a mean annual evapotranspiration (Fig. 6) of 1608.5, 721.5, and 953.5 mm at the Hawassa, Kofele and Wateraressa stations, respectively.

The conventional methods used in previous studies [4,21,41] to represent the spatial distribution of rainfall have mainly depended on the Thiessen polygon. These conventional methods are prone to error propagation in areas within a watershed that are sparsely represented by rain gauge stations, as is the case with the Tikur-Wuha watershed.

As Fig. 7 shows, the map prepared from the merged product obtained by combining CHIRP and rain gauge records (Fig. 7(A)) is considerably different from the areal rainfall map created employing the Thiessen polygon (Fig. 7(B)) for the four rain gauge stations. This type of map discrepancies can have a huge impact on hydrological simulations. Improved spatial rainfall records or representations would significantly enhance the accuracy of recharge estimations, recharge being directly proportional to rainfall. The improvement is indicated by the sharp edges of the recharge map (Fig. 13), similar to the grids of CHIRP-based SREs and the rainfall zones produced by the Thiessen polygon (Fig. 7). The sections that follow provide additional details on the effects of each model input.

4.2. Land use/cover classification

How the sensitivity of recharge estimations can be influenced by land-use maps has been the subject of several previous studies [3,4], which have found that the careful consideration of land-use map could enhance the sensitivity of recharge estimations. Hence, after considering the influence of the sensitivity of recharge estimations on land-use maps, a land-use map of the study area (Fig. 8) was developed for the year 2014. The training and validation accuracies achieved for land-use classification were 0.965 and 0.864 respectively.

As Table 4 indicates, cropland covers the largest proportion (46.72 %) of the total area of the watershed, while 21.35 % of this area is covered by mixed forest. According to the land classification performed by Mohammed et al. (2020), in the year 2017, 46.6 % and 23.6 % of the total area of the watershed were cultivated land and forest cover, respectively [27]. Abraham et al. (2022) found that in the year 2017, 58.62 % and 25.5 % of the watershed area were covered by cultivations and forest [4].

4.3. Model calibration

The model calibration was performed at the Dato-village and Wosha stream gauge stations. A widely accepted practice is to

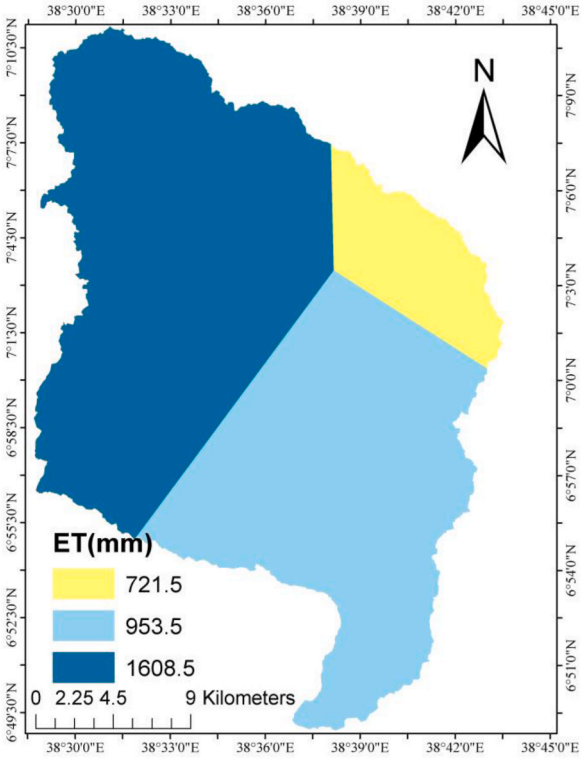

Fig. 6. Mean annual evapotranspiration from the study area.

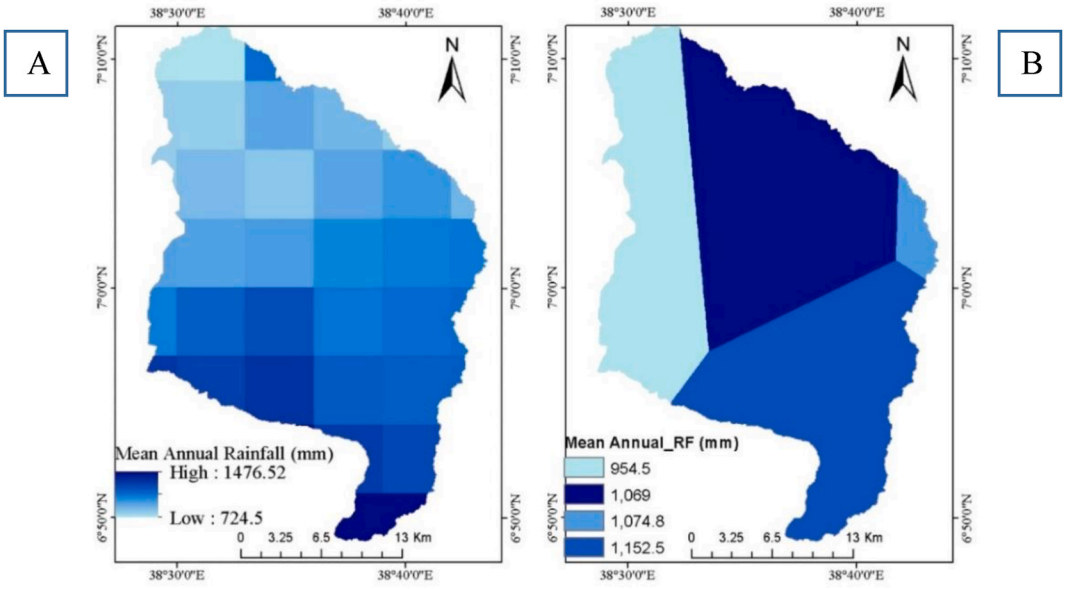

Fig. 7. Mean annual rainfall distribution for the (B) M_1 and (A) M_2 model setups.

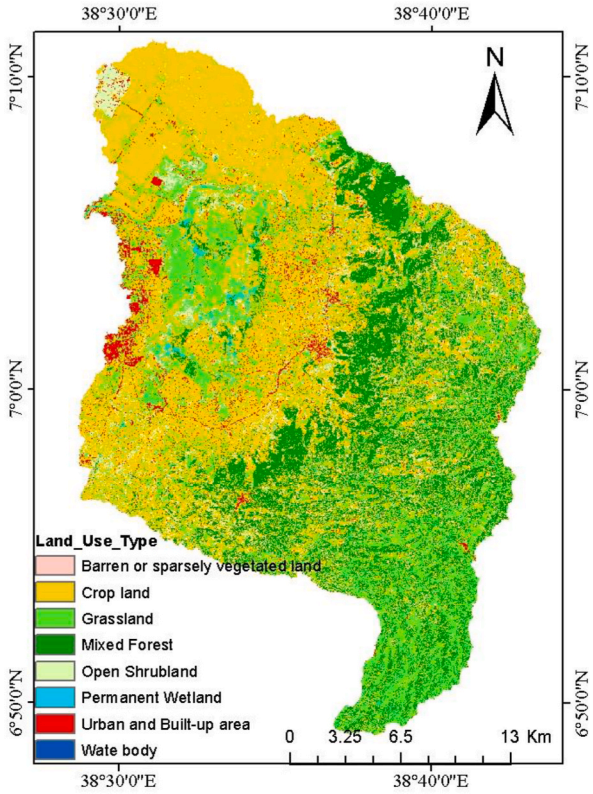

Fig. 8. Land-use map of the Tikur-Wuha watershed prepared for the year 2014.

calibrate a given model using multiple gauge data. Stream gauge data are available at the outlet of the Tikur-Wuha river and its tributaries. Hence, in this study, the model calibration was performed using the gauge records of the Tikur-Wuha river outlet and the data collected from a tributary located downstream of the Wosha subwatershed. Nevertheless, the NSE (0.28) of the calibration performed at the Dato-village station was poor. To improve the calibration results of the Dato-village station, possible parameter

Table 4
Confusion matrix of each land-use class with its percentage coverage area.

Land_Use_Type	Code	12	17	10	11	5	13	16	7	Percent
Crop land	**12**	91	0	1	0	0	1	0	0	**46.72**
Water body	**17**	0	11	0	1	0	0	0	0	0.005
Grassland	**10**	2	0	49	0	0	0	0	0	**19.14**
Permanent wetland	**11**	0	0	2	19	0	0	0	0	1.520
Mixed forest	**5**	0	0	0	1	37	0	0	0	**21.35**
Urban and built-up area	**13**	3	0	1	0	0	44	0	1	3.239
Barren or sparsely vegetated land	**16**	1	0	0	0	0	0	3	0	0.138
Open shrub land	**7**	1	0	1	0	0	0	0	31	7.885

combinations were explored. Additionally, the implementation of strategies such as removing peak values from the observed discharge time-series data and changing the simulation time periods were investigated. However, the maximum NSE obtained was 0.28. By contrast, the NSE of the calibration made at the hydrological station, located downstream of Wosha, was 0.56. Despite the calibration discrepancies, no attempt was made to transfer the calibration results obtained from the Wosha subwatershed gauge station to the Tikur-Wuha watershed gauge station.

The estimated long-term mean annual recharge obtained from the semidistributed simulation model with parameters calibrated for the Wosha subwatershed, was 218.29 mm. The long-term mean annual recharge obtained using the fully distributed simulation model with similar parameters ranged from 0.24 to 579.96 mm. In Fig. 4, a significant mismatch can be observed between the measured stream records obtained from the two discharge gauging stations. Another significant variation is difference in the range of recharge obtained from model parameter calibration using the two discharge records.

The runoff in the study area increases as the recharge rate decreases (Fig. 9) according to the results of the model calibrated using Wosha discharge data; the mean discharge is three times the mean discharge measured at the Dato-village station. Ayenew and Tilahun (2008) argued that fault structures significantly enhance the recharge at the floor of a caldera [23]. Another argument is that the contribution made by the wetland to watershed water balance cannot be disregarded when assessing the recharge [4]. In depicting the effects of various land-use classes on water balance component modeling, implementing separate values for the local parameters of each land-use class would be helpful. The WetSpa model uses permanent wetland, a main land cover class, to calculate the local parameter values. Thus, the impact of wetland on the simulated recharge was properly considered. The WetSpa model does not

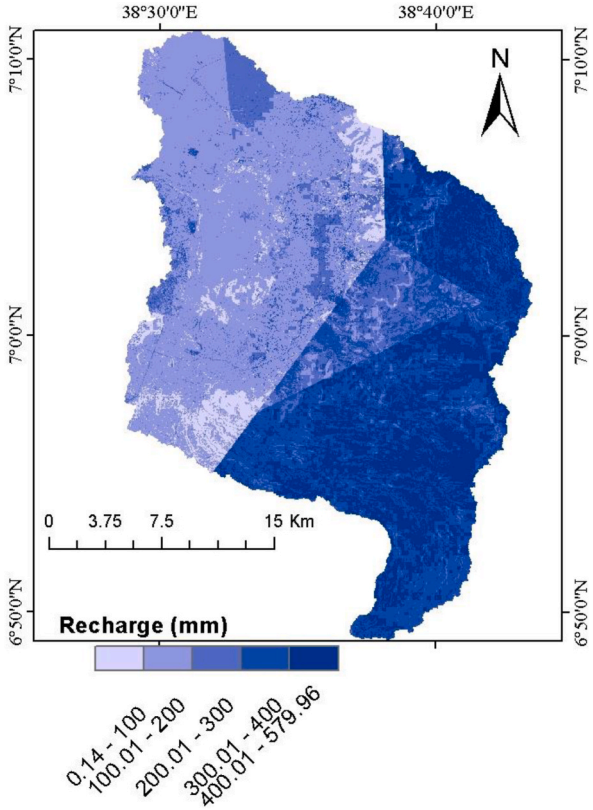

Fig. 9. Long-term mean annual recharge in the study area obtained using Wosha station records.

considers point recharge and/or wetland contribution to recharge as concentrated seepage through existing fault structures. This limitation can cause recharge estimation challenging.

The discrepancies between the recharge magnitudes obtained from the two models calibrated using the Wosha and Dato-village records can be attributed to several factors. However, while the magnitude of recharge rises in an effort to match the discharge size at Dato-village, it falls as the flow rate at Wosha station is more accurately estimated. Because fault structures exist between the two record stations, point recharges can therefore be considered the primary sources of recharge.

4.4. Recharge uncertainty

4.4.1. Semidistributed model simulation

As already explained, the difference between the M_1 and M_2 model setups is in their input rainfall datasets. Thus, land-use local parameters, soil hydraulic parameters, meteorological input datasets used in each model run are same except for the rainfall time-series data. In obtaining the merged rainfall dataset, the original cell size of the CHIRP-based SRE was considered for all rainfall regions. The resulting map had 37 raster cells (0.05° x 0.05°) with own rainfall records. Each grid cell center was assumed to have its own station record, which was fed to the simulation model.

The M_1 model set up that simulated 10,000 parameter combinations, produced a mean annual recharge in the range of 392.03–549.3 mm, whereas semidistributed M_2 model simulating 10,000 parameter combinations produced a mean annual recharge in the range of 316.4–474.9 mm. The results indicate the impacts of input rainfall estimation uncertainties. The large difference between the minimum and maximum simulated recharge values indicates the uncertainty of recharge estimates.

The iteration results obtained from the M_1 model setup demonstrated that both RMSE (Fig. 10(d)) and model volume error (MVE) (Fig. 10(c)) increased as the mean annual recharge increased (Fig. 10). The iteration results of the M_2 model set up show that RMSE (Fig. 10(b)) increases and MVE (Fig. 10(a)) decreases as the mean annual recharge increases; condensed values can be seen in the middle sections of the plots. The RMSE values obtained for 10,000 simulations performed using the M_2 and M_1 setups were in the ranges of 0.8–2.57 m^3/s and 0.8–3.27 m^3/s, respectively.

The results obtained from both model setups indicated that the long-term mean annual recharge was in the range of 370–430 mm. The RMSE values obtained from the M_1 model setup are densely distributed at low values of the long-term mean annual recharge, while the RMSE values obtained from the M_2 model setup are dispersed at the beginning and end of the X-axis depicting long-term mean annual recharge values. An exhaustive search of random parameter combinations that will ensure performance measure convergence, guided by a literature review and expert knowledge of the hydroclimatic characteristics of the watershed have helped to explore the global ranges of each parameter. This predefined ranges of the parameter values were used at the start to randomly generate possible parameter combinations. The use of Monte Carlo simulation in conjunction with Latin Hypercube Sampling to generate possible parameter combinations has helped to ensure that the parameters were properly distributed in the given parameter space.

The plot of evapotranspiration coefficient (K-ep) against recharge (Fig. 11) shows an inverse correlation between the mean annual recharge and K-ep; that is, the mean annual recharge decreases as K-ep increases. As K-ep increases, PVE also increases. This

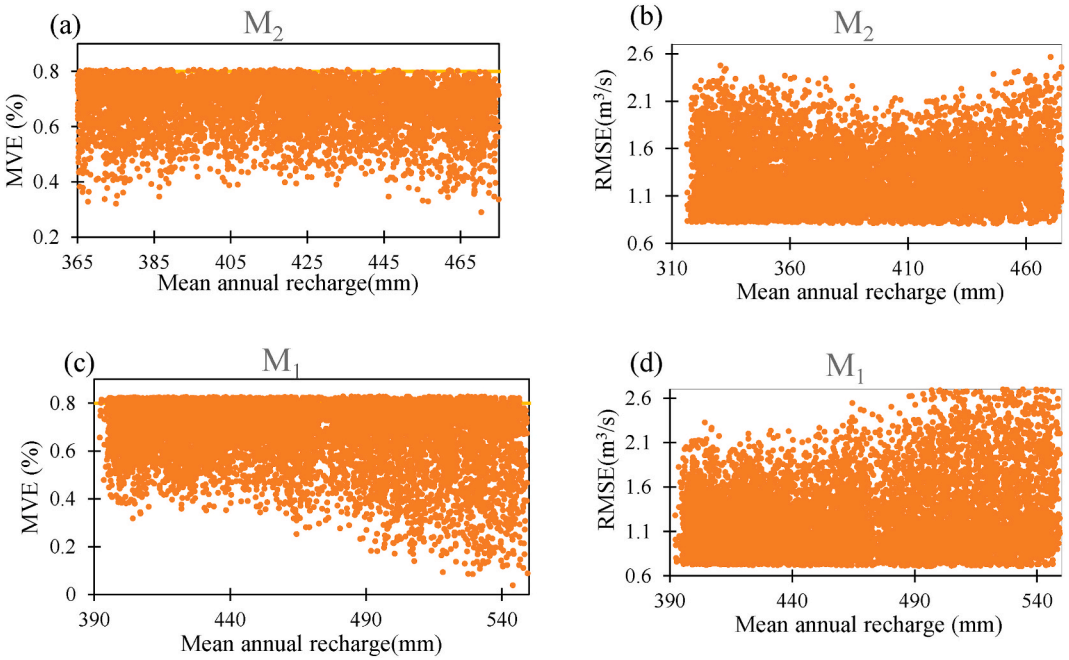

Fig. 10. PVE and RMSE values obtained for 10,000 model realizations using M_1 (c & d) and M_2 (a & b) model setups.

correlation indicates the importance of obtaining accurate evapotranspiration estimates. Thus, we can conclude that improved estimates of evapotranspiration can reduce the uncertainty of recharge estimations.

4.4.2. Fully distributed simulation

The fully distributed simulation model available with the WetSpa extension generates the recharge accumulated in a targeted basin over the simulation period, taken as 10 years in this study. The average of the long-term recharge obtained from 100 best spatial recharge maps produced by the M_1 model set up (Fig. 12 (A)) is significantly different from that generated using the M_2 model setup. The model outputs depend on the input rainfall maps. Additionally, the highest and lowest long-term mean recharge is different for M_1 and M_2, where recharge estimates of M_2 are greater than M_1. CHIRP-based SREs are noted for their overestimated rainfall values [13, 17], which have been reflected in the highest recharge estimate produced by the M_2 model setup. According to Beyene et al. (2023), the raw CHIRP rainfall estimates show a false alarm ratio as high as 50 %, indicating a noticeable increase in the depth of estimated rainfall values. Various bias correction techniques can be applied to reduce the inaccuracies present in volume estimations. A multistage bias correction strategy [35] has improved the PVE of CHIRP-based SREs by up to 70 %. The overestimation can be decreased by using other bias correction techniques available. The two images shown below indicate the substantial spatial heterogeneity of the two standard deviation (STDEV) maps (Fig. 12).

Another strategy used to analyze the uncertainty in recharge estimations was to observe the STDEV of the selected 100 model realizations obtained from each model setup. A low STDEV indicates low uncertainty, while a high STDEV indicates high uncertainty in the estimations. The results show that merged SREs produce recharge maps with low uncertainty. The plots pertaining to the M_1 model setup shown on the left (Fig. 12(A)) indicate a maximum STDEV of 1156.25 mm with most of the areas in the study area having high STDEV values. The plots pertaining to the M_2 model set up (Fig. 12(B)) exhibit the highest STDEV in a small part of the watershed. The M_1 model setup plots indicate that most areas of the watershed have high values of uncertainty.

By dividing the long-term average recharge by 10, the number of years in the simulation period, the mean annual long-term recharge map of the study area can be obtained (Fig. 13). From the maps, the impact on recharge magnitudes and spatial distributions due to rainfall and evapotranspiration can be observed. Fig. 13 shows a pattern similar to the Thiessen polygon map (Fig. 6) developed using the evapotranspiration records obtained from monitoring stations. The pattern indicates that evapotranspiration has a significant impact on recharge estimation.

From the long-term mean annual recharge maps shown in Fig. 13, the continuous impact caused by evapotranspiration can be observed. The western flat lands (Fig. 8), dominated by crop land, of the watershed, exhibited a low recharge magnitude (Fig. 13 (A, B)), whereas eastern mountain ranges exhibited high recharge magnitudes.

According to previous studies where similar procedures were followed [7], model calibrations performed to determine possible parameter ranges can decrease the uncertainty in recharge estimations. However, this study relied on uncalibrated parameter ranges, determined based on literature and prior information related to the watershed. Thus, the output recharge map would not indicate the true or near true values of the recharge in the watershed. Nonetheless, the results have illustrated the important role played by spatial rainfall distributions in recharge estimations.

The coefficient of variation (Cv) values obtained from the 100 best recharge maps produced by the M_1 model set up (Fig. 14) indicated more consistent recharge estimations compared with the corresponding values obtained by the M_2 model setup. The highest uncertainty in recharge estimations was observed in the wetland-dominated part of the watershed. Abraham et al. (2022) also observed a similar high recharge variability in the wetland-dominated part of the watershed [4]. Seventy percent of the watershed showed a $Cv < 0.15$ for the M_2 model setup (Fig. 14(B)), while 90 % of the watershed exhibited a $Cv < 0.15$ for the M_1 model setup (Fig. 14(A)).

The recharge estimation sensitivity was studied by Abraham et al. (2022) using the calibrated soil water assessment (SWAT) tool SWAT-Cup, and the median recharge for the year 2017 was found to be in the range of 397–575 mm [4]. Despite the differences in the model setups, simulation periods, and model structures, significant variations can be observed between the recharge zone results of Abraham et al. (2022) and those of this study. According to Abraham et al. (2022), the wetland-dominated central part of the watershed exhibited a high median recharge, whereas this study showed that it had a low median recharge [4]. The estimated median recharge was low in the eastern mountainous parts of the watershed [4]. The semidistributed simulation performed in this study using the M_1 model setup produced a mean annual recharge between 392.03 and 549.3 mm.

5. Conclusions

Accurate modeling of all hydrological cycle components is necessary to ensure sustainable water resources management. The developments in satellite technology throughout the past few decades have played a significant role in the observation and measurement of several meteorological parameters. Additionally, the benefits of merging different techniques to gain advantage of the merits of each technique are increasing. Considering the direct relationship between recharge and rainfall records, the uncertainties in recharge estimations due to rainfall data uncertainties were assessed in this study.

The physically based distributed hydrological model WetSpa was used to simulate over 20,000 possible model parameter combinations. Ten thousand of these simulations were run using rain gauge-based records, while the remaining simulations were run using CHIRP-based SREs that had been bias corrected and combined with the available rain gauge records. All other meteorological data and physiographical data used as model inputs were kept constant except for rainfall data. The results demonstrated that improved spatial representation of the rainfall increases the accuracy of spatial recharge estimations. Additionally, the results showed that the spatial representation of evapotranspiration can have a significant impact on the estimations of long-term recharge distribution.

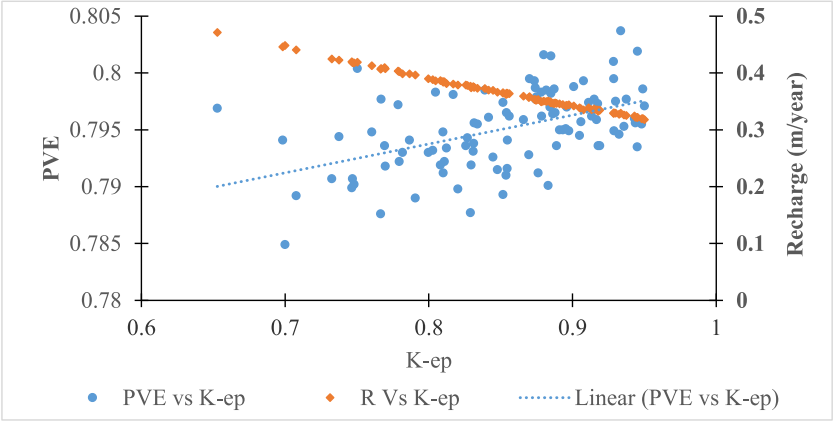

Fig. 11. Correlation between the evaporation coefficient (K-ep) and percentage volume error (PVE) of the estimated mean annual recharge (R) for the 100 best parameter combinations.

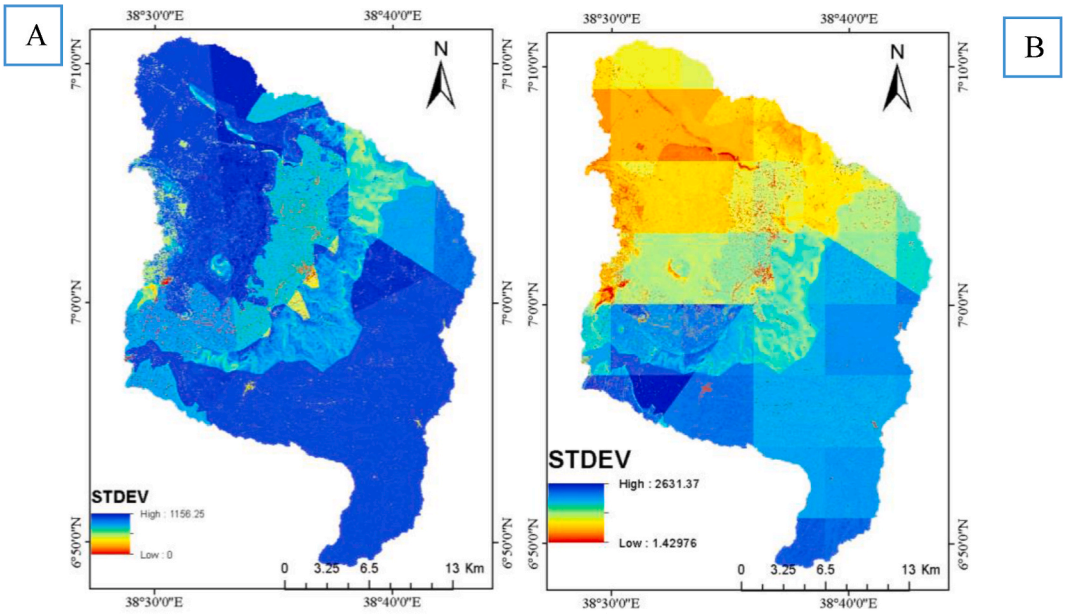

Fig. 12. Standard deviations of the 100 model realizations produced by M_1 (A) and M_2 (B) model set ups.

Limitations were encountered in examining point recharges through faults and direct recharge from uncontrolled irrigation fields dispersed throughout the watershed along with their respective water uses. The use of a customized look-up table for local variables of the WetSpa model was assumed sufficient to overcome the effects of these limitations. Additionally, a literature review revealed that few studies have explored the effects of geological faults on groundwater flow patterns [4,23], groundwater abstraction by large-scale farm lands in the Tikur-Wuha watershed [23], and the total amount of water abstracted for traditional or uncontrolled irrigation practices [46]. However, no previous studies have particularly focused on the quantification of recharge from irrigation fields or point recharges in the fault zones. Hence, the recharges estimated in this study does not reflect the actual recharges of the watershed.

Hence, future studies should consider the direct recharge from irrigation fields, which can be estimated either through field level measurements or by introducing representative parameters to existing hydrogeological models. Additionally, the determination of point recharges through fault structures using methods such as modified chloride mass balance approach, could be considered in future studies. Furthermore, precise spatial evapotranspiration estimation should be explored in future to reduce its influence on recharge estimation uncertainty.

6. Data availability Statement

Data can be made available on request.

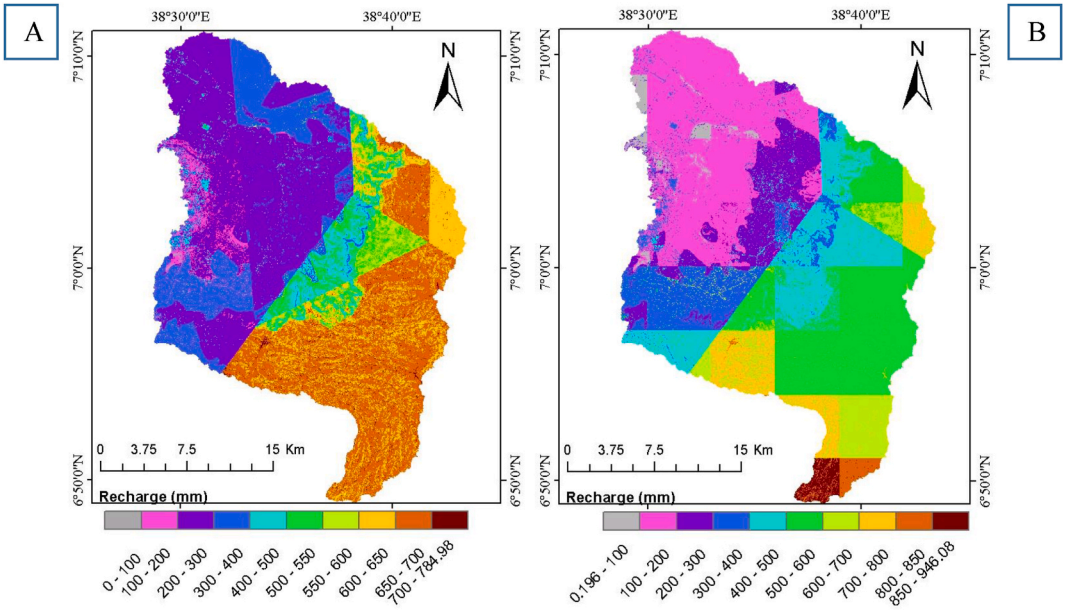

Fig. 13. Long-term mean annual recharge map of M_1 (A) and M_2 (B) model setups.

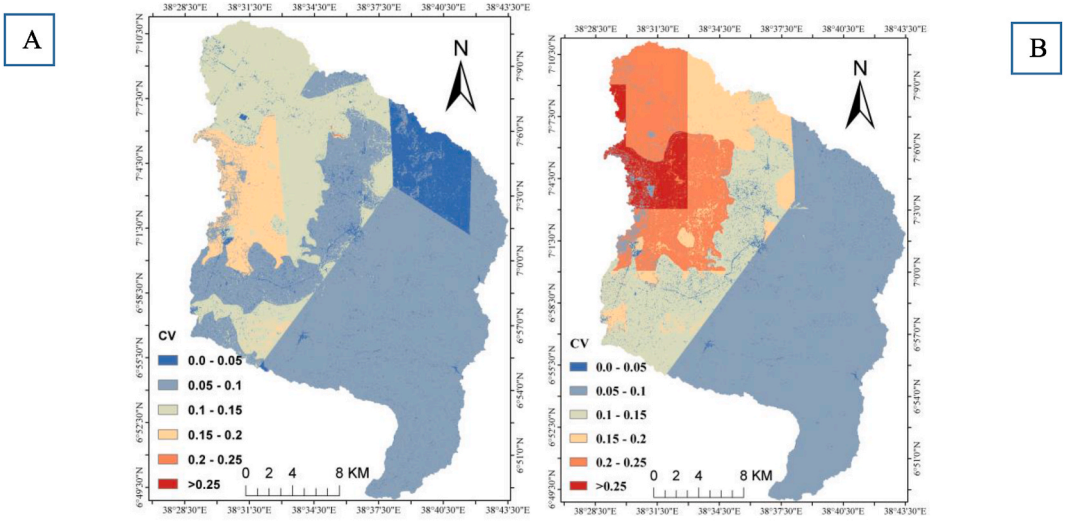

Fig. 14. Coefficient of variation of the study area obtained from (A) M_1 and (B) M_2 model setups.

CRediT authorship contribution statement

Tsegamlak Diriba Beyene: Writing – original draft, Visualization, Validation, Software, Methodology, Investigation, Formal analysis, Data curation, Conceptualization. **Fasikaw Atanaw Zimale:** Writing – review & editing, Validation, Supervision, Software, Resources, Methodology. **Sirak Tekleab Gebrekristos:** Writing – review & editing, Validation, Supervision, Resources, Methodology. **Dessie Nedaw:** Writing – review & editing, Validation, Supervision, Resources, Methodology.

Declaration of competing interest

The authors declare that they have no known competing financial interests or personal relationships that could have appeared to influence the work reported in this paper.

Acknowledgments

This study was supported by Africa Center of Excellence for Water Management (ACEWM), Addis Ababa University. We are appreciative of all the help ACEWM provided during the study. We express our gratitude to Mr. Ashenafi A. Gemechu for his assistance during the language editorial process.

References

[1] E. Moges, Y. Demissie, L. Larsen, F. Yassin, Sources of hydrological model uncertainties and Advances in their analysis, Water 13 (1) (2021) 28.
[2] F. Manna, S. Murray, D. Abbey, P. Martin, J. Cherry, B. Parker, Spatial and temporal variability of groundwater recharge in a sandstone aquifer in a semiarid region, Hydrol. Earth Syst. Sci. 23 (4) (2019).
[3] E.M. Ampe, I. Vanhamel, E. Salvadore, J. Dams, I. Bashir, L. Demarchi, J.C.-W. Chan, H. Sahli, F. Canters, O. Batelaan, Impact of urban land-cover classification on groundwater recharge uncertainty, IEEE J. Sel. Top. Appl. Earth Obs. Rem. Sens. 5 (6) (2012) 1859–1867.
[4] T. Abraham, A. Muluneh, R. Girma, A. Hartmann, S. Tekleab, Quantifying sensitivity of groundwater recharge to land use and land cover changes by improving model performance on the wetland dominated Tikur Wuha watershed, Ethiopia, Water Cycle 3 (2022) 112–125.
[5] Z. Zomlot, B. Verbeiren, M. Huysmans, O. Batelaan, Trajectory analysis of land use and land cover maps to improve spatial–temporal patterns, and impact assessment on groundwater recharge, J. Hydrol. 554 (2017) 558–569.
[6] E.A. Baker, A. Cappato, S. Todeschini, L. Tamellini, G. Sangalli, A. Reali, S. Manenti, Combining the Morris method and multiple error metrics to assess aquifer characteristics and recharge in the lower Ticino Basin, in Italy, J. Hydrol. 614 (2022) 128536.
[7] Y. Xie, P.G. Cook, C.T. Simmons, D. Partington, R. Crosbie, O. Batelaan, Uncertainty of groundwater recharge estimated from a water and energy balance model, Journal of hydrology 561 (2018) 1081–1093.
[8] Y.T. Dile, E.K. Ayana, A.W. Worqlul, H. Xie, R. Srinivasan, N. Lefore, L. You, N. Clarke, Evaluating satellite-based evapotranspiration estimates for hydrological applications in data-scarce regions: a case in Ethiopia, Sci. Total Environ. 743 (2020) 140702.
[9] Z. Duan, Y. Tuo, J. Liu, H. Gao, X. Song, Z. Zhang, L. Yang, D.F. Mekonnen, Hydrological evaluation of open-access precipitation and air temperature datasets using SWAT in a poorly gauged basin in Ethiopia, Journal of hydrology 569 (2019) 612–626.
[10] P. Nasta, J.B. Gates, Y. Wada, Impact of climate indicators on continental-scale potential groundwater recharge in Africa, Hydrol. Process. 30 (19) (2016) 3420–3433.
[11] A. Mechal, T. Wagner, S. Birk, Recharge variability and sensitivity to climate: the example of gidabo river basin, main Ethiopian rift, J. Hydrol.: Reg. Stud. 4 (2015) 644–660.
[12] T. Turkeltaub, G. Bel, The effects of rain and evapotranspiration statistics on groundwater recharge estimations for semi-arid environments, Hydrol. Earth Syst. Sci. 27 (1) (2023) 289–302.
[13] T. Dinku, P. Ceccato, S.J. Connor, Challenges of satellite rainfall estimation over mountainous and arid parts of east Africa, Int. J. Rem. Sens. 32 (21) (2011) 5965–5979.
[14] G.B. Adane, B.A. Hirpa, C.-H. Lim, W.-K. Lee, Evaluation and comparison of satellite-derived estimates of rainfall in the diverse climate and terrain of central and northeastern Ethiopia, Rem. Sens. 13 (7) (2021) 1275.
[15] C.K. Omondi, Assessment of Bias Corrected Satellite Rainfall Products for Streamflow Simulation: a TOPMODEL Application in the Kabompo River Basin, Zambia, University of Twente, 2017.
[16] G.B. Adane, B.A. Hirpa, B.M. Gebru, C. Song, W.-K. Lee, Integrating satellite rainfall estimates with hydrological water balance model: rainfall-runoff modeling in awash river basin, Ethiopia, Water 13 (6) (2021) 800.
[17] T. Dinku, K. Hailemariam, R. Maidment, E. Tarnavsky, S. Connor, Combined use of satellite estimates and rain gauge observations to generate high-quality historical rainfall time series over Ethiopia, Int. J. Climatol. 34 (7) (2014) 2489–2504.
[18] G.Y. Ebrahim, J.F. Lautze, K.G. Villholth, Managed aquifer recharge in Africa: taking stock and looking forward, Water 12 (7) (2020) 1844.
[19] Y.T. Dile, S. Tekleab, E.K. Ayana, S.G. Gebrehiwot, A.W. Worqlul, H.K. Bayabil, Y.T. Yimam, S.A. Tilahun, P. Daggupati, L. Karlberg, Advances in water resources research in the Upper Blue Nile basin and the way forward: a review, J. Hydrol. 560 (2018) 407–423.
[20] Q. Hu, Z. Li, L. Wang, Y. Huang, Y. Wang, L. Li, Rainfall spatial estimations: a review from spatial interpolation to multi-source data merging, Water 11 (3) (2019) 579.
[21] A. Lemlem, Assessing the Impact of Land Use and Land Cover Change on Groundwater Recharge Using Rs and Gis; a Case of Awassa Catchement, Southern Ethiopia, Addis Ababa University, 2008.
[22] T. Kifle, A. Deres, A. Birku, T. Aberham, D. Mengist, Evaluation of the impacts of land use and land cover changes using erosion assessment model at Tikur wuha watershed, Evaluation 10 (9) (2020).
[23] T. Ayenew, N. Tilahun, Assessment of lake–groundwater interactions and anthropogenic stresses, using numerical groundwater flow model, for a Rift lake catchment in central Ethiopia, Lakes Reservoirs Res. Manag. 13 (4) (2008) 325–343.
[24] A. Yeneneh, Characterization of Groundwater-Lake Water Interaction in Lake Hawassa Basin, Addis Ababa University, 2014.
[25] S. Kebede, Groundwater occurrence in regions and basins, in: Groundwater in Ethiopia, Springer, 2013, pp. 15–121.
[26] L.B. Zemedagegnehu, Groundwater development and management practices in lake awassa catchment, southern Ethiopia, J. Environ. Earth Sci. 10 (2020).
[27] M. Mohammed, B. Biazn, M.D. Belete, Hydrological impacts of climate change in Tikur wuha watershed, Ethiopian rift valley basin, J. Environ. Earth Sci. 10 (2) (2020) 28–49.
[28] M.D. Belete, B. Diekkrüger, J. Roehrig, Linkage between water level dynamics and climate variability: the case of Lake Hawassa hydrology and ENSO phenomena, Climate 5 (1) (2017) 21.
[29] T. Abraham, A. Muluneh, Quantifying impacts of future climate on the crop water requirement, growth period, and drought on the agricultural watershed, in Ethiopia, Air Soil. Water Res. 15 (2022) 11786221221135151.
[30] T. Abraham, A. Muluneh, Assessing Impacts of Future Climate on the Crop Water Requirement and Growth Period. A Case of Lake Hawassa Watershed, Ethiopia, 2022.
[31] W. Kebede, M. Tefera, T. Habitamu, T. Alemayehu, Impact of land cover change on water quality and stream flow in lake Hawassa watershed of Ethiopia, Agric. Sci. 2014 (2014).
[32] N. Wondrade, Ø.B. Dick, H. Tveite, GIS based mapping of land cover changes utilizing multi-temporal remotely sensed image data in Lake Hawassa Watershed, Ethiopia, Environ. Monit. Assess. 186 (2014) 1765–1780.
[33] A. Degife, H. Worku, S. Gizaw, A. Legesse, Land use land cover dynamics, its drivers and environmental implications in Lake Hawassa Watershed of Ethiopia, Remote Sens. Appl.: society and environment 14 (2019) 178–190.
[34] C. Funk, P. Peterson, M. Landsfeld, D. Pedreros, J. Verdin, S. Shukla, G. Husak, J. Rowland, L. Harrison, A. Hoell, The climate hazards infrared precipitation with stations—a new environmental record for monitoring extremes, Sci. Data 2 (1) (2015) 1–21.
[35] T.D. Beyene, F.A. Zimale, S.T. Gebrekristos, D. Nedaw, Evaluation of a multi-staged bias correction approach on CHIRP and CHIRPS rainfall product: a case study of the Lake Hawassa watershed, Journal of Water and Climate Change 14 (6) (2023) 1847–1867.
[36] T. Enku, A.M. Melesse, A simple temperature method for the estimation of evapotranspiration, Hydrol. Process. 28 (6) (2014) 2945–2960.
[37] S.H. Hasan, A.N. AL-Hameedawi, H. Ismael, Supervised classification model using Google Earth engine development environment for wasit governorate, in: IOP Conference Series: Earth and Environmental Science, IOP Publishing, 2022.
[38] H.C. Kraemer, Kappa Coefficient, Wiley StatsRef: statistics reference online, 2014, pp. 1–4.

[39] Y. Liu, F. De Smedt, WetSpa Extension, a GIS-Based Hydrologic Model for Flood Prediction and Watershed Management, vol. 1, Vrije Universiteit Brussel, Belgium, 2004, p. e108.
[40] A. Yenehun, M. Dessie, F. Nigate, A.S. Belay, M. Azeze, M. Van Camp, D.F. Taye, D. Kidane, E. Adgo, J. Nyssen, Spatial and temporal simulation of groundwater recharge and cross-validation with point estimations in volcanic aquifers with variable topography, J. Hydrol.: Reg. Stud. 42 (2022) 101142.
[41] A. Yenehun, F. Nigate, A.S. Belay, M.T. Desta, M. Van Camp, K. Walraevens, Groundwater recharge and water table response to changing conditions for aquifers at different physiography: the case of a semi-humid river catchment, northwestern highlands of Ethiopia, Sci. Total Environ. 748 (2020) 142243.
[42] A. Bahremand, WetSpa model application with and without calibration, in: EGU General Assembly Conference Abstracts, 2018.
[43] S. Kidanemariam, H. Goitom, Y. Desta, Coupled application of R and WetSpa models for assessment of climate change impact on streamflow of Werie Catchment, Tigray, Ethiopia, Journal of Water and Climate Change 12 (3) (2021) 916–936.
[44] A. Bahremand, Opinions Hess, Advocating process modeling and de-emphasizing parameter estimation, Hydrol. Earth Syst. Sci. 20 (4) (2016) 1433–1445.
[45] D.R. Legates, G.J. McCabe Jr., Evaluating the use of "goodness-of-fit" measures in hydrologic and hydroclimatic model validation, Water Resour. Res. 35 (1) (1999) 233–241.
[46] Y. Teshome, B. Biazin, K. Wolka, A. Burka, Evaluating performance of traditional surface irrigation techniques in Cheleleka watershed in Central Rift Valley, Ethiopia, Appl. Water Sci. 8 (2018) 1–14.